Available online at www.sciencedirect.com
ScienceDirect
Trans. Nonferrous Met. Soc. China 29(2019) 485−494
Transactions of Nonferrous Metals Society of China
www.tnmsc.cn

Formation and elimination of burst phenomenon in ultrasonic-assisted resistance brazing

Wei-yuan YU[1], Tian-yu ZHANG[1,2], Yu WANG[2], Meng-zhao GAO[1], Jiang-xu SHANG[1], Ze-hua YAN[1], Wei-jie WU[1], Qiao-li LIN[1]

1. State Key Laboratory of Advanced Processing and Recycling of Non-Ferrous Metals, Lanzhou University of Technology, Lanzhou 730050, China;
2. State Key Laboratory of Rolling and Automation, Northeastern University, Shenyang 110819, China

Received 26 January 2018; accepted 26 December 2018

Abstract: A two-step ultrasonic-assisted brazing method and its associated apparatus were developed to make 6063 aluminum alloys joints with Al−Si−Mg filler metal. The burst phenomenon and the effect of ultrasonic direction and time, as well as the welding joint geometry on the burst phenomenon were investigated. The results show that the burst phenomenon occurs in the liquid filler metal under the effects of high current density, heat, and interaction force. The burst phenomenon is eliminated when the oxide film on the edge of the cross-section of the two parent metals is removed with more than or equal to 6 s ultrasonic time. A model of formation and elimination for burst was proposed, through which the blasting phenomenon can be controlled by changing the ultrasonic time and the geometrical shape of the welded joint.

Key words: 6063 aluminum alloys; ultrasonic-assisted brazing; resistance brazing; burst

1 Introduction

The high-productivity, rapid-heating resistance brazing technique is widely used to join the dissimilar alloy and the similar alloy [1−3], owing to the low impact of concentrated heat treatment on the thermal characteristics of the base metal. And the well-brazed area of the resistance brazing joint interface increased by more than 35% (up to 85%) because ultrasonic vibration was applied [1]. In addition, a novel “two-step resistance brazing method” was presented [2]. TANAKA et al [4] performed a numerical simulation of the welding process for the two-step resistance brazing method. In their studies, the first step of this method improved the uniformity of the contact conditions between the two surfaces and promoted the optimal energizing conditions for the second resistance brazing step. Ultrasonic vibration and resistance brazing has been combined to join Al [5], Al matrix composites [6], and Mg alloys [7]. Particularly, WEIS et al [6] investigated the surface pressure, transformer and ultrasonic performance, and different joining surface geometries, which affect the joint properties. Previous works mainly focused on joining of the smaller-specimen materials, improvement of bond strength and removing of pores and the unmelted solder in the brazing seam, while the mechanism of ultrasonic-assisted resistance brazing was seldom discussed.

The aluminium alloys are widely used in automotive applications because of low density, excellent formability and corrosion resistance. In the research of resistance spot welding of Al alloy, a welding current approximately up to 30 kA was used to achieve a good welding joint [8]. ZHENG et al [9] reduced the welding current by about 20% and improved the quality of welding nugget with a large resistance medium; however, the current used was still relatively large. Recently, we have found that ultrasonic-assisted resistance brazing could achieve a good welding effect by using a smaller current of approximately 5 kA.

Ultrasonic vibration has been found to remove surface oxides and impurities from particles, promote heterogeneous nucleation, and refine the grain size in the α-phase [10−12]. The mechanical effect of the ultrasonic vibration promoted the elements in the joint composition

Corresponding author: Tian-yu ZHANG; Tel: +86-24-83690363; E-mail: zhangty12359@sina.com
DOI: 10.1016/S1003-6326(19)64957-5

to assume a uniform distribution and caused a mutual penetration of the molecules [13,14]. The ultrasonic energy applied to the liquid phase promoted the dissolution of the base material [15−19], which could influence the metallurgical reaction behaviour of the solid−liquid interface [20]. The stirring effect of the ultrasonic treatment promoted atomic diffusion at the solid−liquid interface [21] and reduced the precipitate deposition at the interface [13].

In this study, the two-step ultrasonic-assisted resistance brazing method with a novel ultrasonic welding apparatus was developed to braze Al alloy. Furthermore, the mechanism for the formation and elimination of the burst phenomenon and the variation of the current path in the ultrasonic-assisted resistance brazing process were investigated. The effects of the ultrasonic direction and time, as well as the welding joint geometry on the burst phenomenon were studied.

2 Experimental

The experimental apparatus consisted of a spot welding machine, an ultrasonic vibration module, and a fixture apparatus. A DT-40-type AC spot welding machine was selected for the welding power supply.

Figure 1 shows the fixture apparatus, comprising a slide guide, string, insulator, pilot pin, and weight. The aluminium plate installed above the slide guide could move vertically. The string, pilot pin, and weight unit can easily set and modify the welding stress as required. A filler metal piece is inserted between the facing surfaces of the two aluminium plates, and stress can be applied via the weight and string.

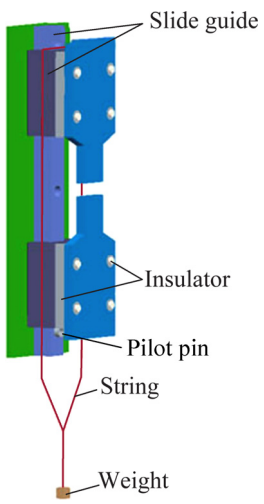

Fig. 1 Schematic of fixture apparatus

The development of the welding parameters about the current and force is shown in Fig. 2. Ultrasonic-assisted resistance brazing is divided into two steps: the first is a low current treatment, and the second is a higher current treatment combined with ultrasonic vibration. Al alloy plates of 8 mm were welded with the butt joints, and the welding sizes were 20 mm×8 mm. The Al−Si−Mg filler with dimensions of 18 mm×6 mm×0.3 mm was located between the two parts to be joined. Surfaces to be bonded were mechanically polished to a 240-grit finish and then ultrasonically degreased in acetone. Under the alternating current (AC) conditions, the heat at locations CR (between the filler metal and the base metal) and IR (the filler metal) was much higher. The filler metal was melted by the heat generated from the current, after which the filler metal reacted with the base metal rapidly. Then an ultrasonic wave with the amplitude of 15 μm and a frequency of 20 kHz was applied to the perpendicular beam of the samples for 0−10 s, which is shown in Fig. 3. Welding procedure and joint geometry conditions used in this experiment are shown in Table 1. The welding procedure during the resistance brazing is defined as (2.5 kA, 1 s)+(5.5 kA, x s), where time x is 5, 10 and 20 s. The microstructure of filler metal is observed by planar and grooved joints, and a grooved joint with a size of 0.15 mm is added to the weld joint of the base metal to prevent excessive filler metal outflow from the seam.

The fusion parameters of the Al−Si−Mg filler metal (the solidus and liquidus temperatures) were measured

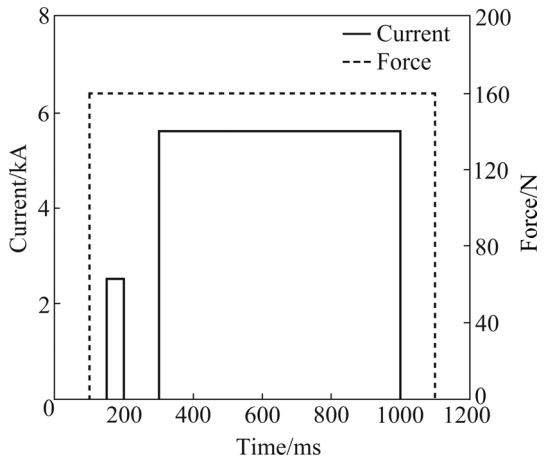

Fig. 2 Development of weld parameters: current (solid line) and force (dotted line)

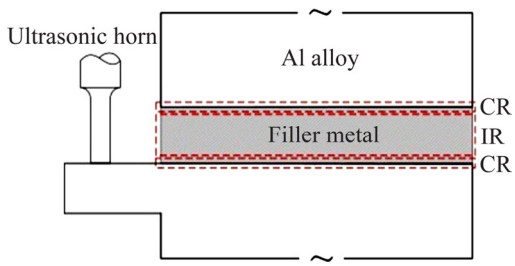

Fig. 3 Schematic diagram of resistance brazing process with ultrasonic wave (CR — Contact resistance; IR — Internal resistance)

Table 1 Welding procedure and joint geometry

Condition	Welding procedure	Joint geometry
I	(2.5 kA, 1 s)+(5.5 kA, 5 s)	Planar
II	(2.5 kA, 1 s)+(5.5 kA, 10 s)	Planar
III	(2.5 kA, 1 s)+(5.5 kA, 20 s)	Planar
IV	(2.5 kA, 1 s)+(5.5 kA, 5 s)	Grooved
V	(2.5 kA, 1 s)+(5.5 kA, 10 s)	Grooved
VI	(2.5 kA, 1 s)+(5.5 kA, 20 s)	Grooved

by differential thermal analysis (DTA). The interfacial microstructure of the samples was observed using an optical microscope (OP MEF−3), and a scanning electron microscope (SEM, Quanta FEG 450) equipped with an energy dispersive X-ray spectrometer (EDS) analysis system.

3 Results and discussion

3.1 Occurrence of burst phenomenon

Figure 4 shows the microstructures of the resistance brazing welded joints under condition III without ultrasonic treatment. Many cavities were observed in the longitudinal direction and the width of the weld varied in the brazed joint (Fig. 4(a)). Interestingly, the burst phenomenon occurred during the welding process. A large amount of filler metal was squeezed out of the brazing seam accompanied with the occurrence of the burst phenomenon. A magnified image of the planar surface of the brazed joint is shown in Fig. 4(b) and the phases are identified by EDS. The acicular structure is the Si phase, the grey areas found in the filler metal represent the primary α(Al) phase, and the dark grey regions represent the Al−Si−Mg eutectic phase. The brazed joint consisted of a columnar primary α(Al) phase oriented perpendicular to the growth of the base metal, dendritic primary α(Al) phase located in the centre of the weld, Al−Si−Mg eutectic structure, and acicular Si [22]. Figure 4(c) shows the corresponding EDS map of Si in Fig. 4(a), which indicates that the Si is distributed at the grain boundaries of the primary α(Al) phase along the direction of the current.

By controlling the current time of the second step, the melting process of filler metal and the variation of the current path during welding are explored. Figure 5 shows the microstructures of the joint under condition I. Considering the whole welding process, a large number of holes were generated at the interface between the filler metal and base metal because the instantaneous large current (the initial currents of the first and second stages) passing through the close contact region. The contact resistance and the current density in this region were greater than those of the base metal and the filler metal at

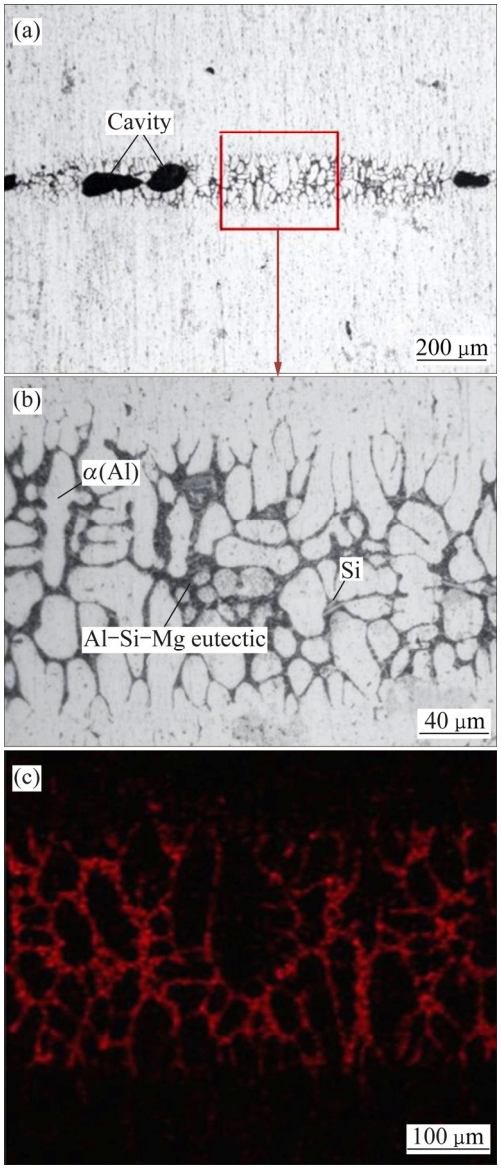

Fig. 4 OM images of resistance brazing welded joint under condition III: (a) Microstructure of bonds; (b) Local magnification of zone in (a); (c) Corresponding EDS map of Si

the initial stage of welding process [23], and the heat generated by the contact resistance was enough to cause some filler metal to vaporise. The holes formed during cooling. High magnification image of the brazed joint (Fig. 5(b)) shows that the oxide film at the interface was removed under the action of the alternating current (AC) and heat, with only a small amount of discontinuous oxidation film observed at the interface.

When the second phase current was extended, the burst phenomenon occurred during the process. Figure 6 shows the microstructure of the joints obtained by condition II. Overall, the width of the entire welding line is uneven, with the widest and narrowest weld widths about 650 and 160 μm, respectively (Fig. 6(a)). The reaction rates between filler and base metals made the uneven weld heat, resulting in the change of weld

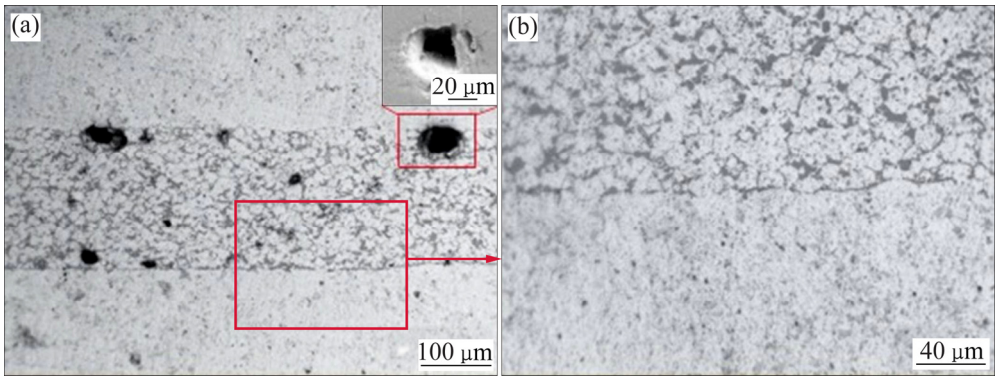

Fig. 5 OM images of joint under condition I: (a) Microstructure of bonds; (b) Local magnification of zone in (a)

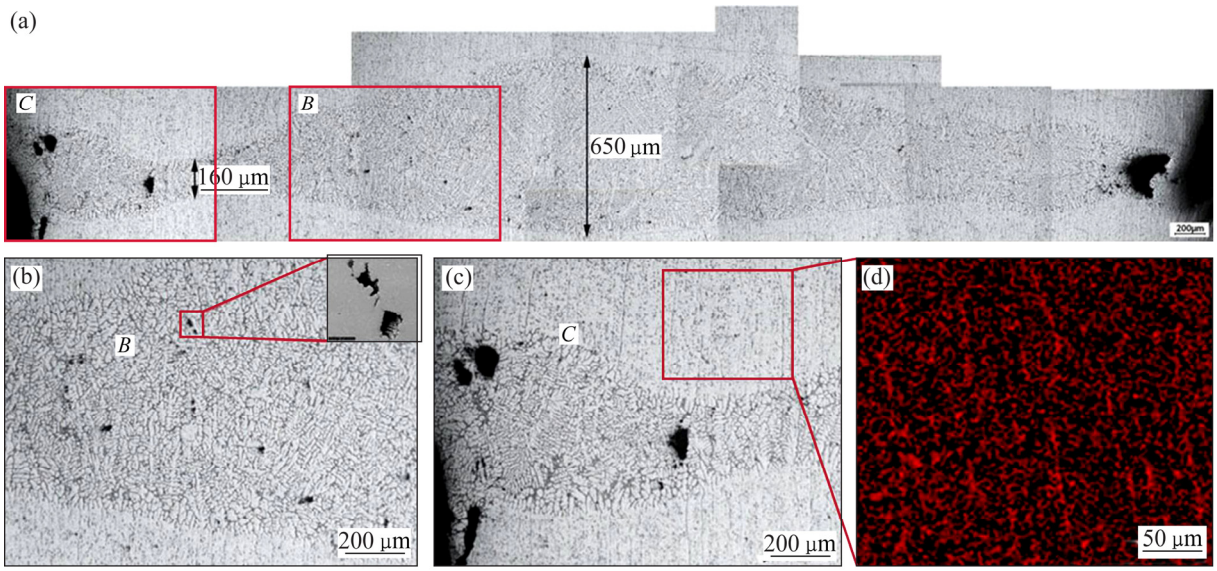

Fig. 6 OM images of resistance brazing welded joint under condition II: (a) Microstructure of bonds; (b, c) Local magnification of zone in (a); (d) Corresponding EDS map of Si in (c)

width. Equation (1) describes the Joule heating effect associated with the welding process, where Q is the input energy, R is the total resistance, I is the input current, and t is the total welding time.

$$Q=I^2Rt \tag{1}$$

As the resistance and treatment time are kept constant throughout the experiment and the heating effect is mainly determined by the amplitude of the current in the weld, it can be inferred that a change in the current path caused the inhomogeneous heat distribution. Figure 6(b) shows that many irregular hole shapes formed, which varied with the phase in which the hole is situated, and the primary Al phase dendrites present around it. Therefore, the heat reached the melting point of the filler metal and the holes formed because of the overreaction between the filler and base metals and expansion and contraction. Analysis of the ends of the cross section by EDS revealed that silicon diffused into the base metal via the Al grain boundaries parallel to the direction of the current (Figs. 6(c, d)). Point scanning analysis on the ends of the sample showed that the local Si content was as high as 7.8 wt.%, therefore, the Si element came mostly from the filler metal. Under the high temperature conditions, with a large amount of heat produced under the current action, Si spread rapidly via the Al grain boundaries. Therefore, it can be concluded that most of the current flowed through the ends of the cross-section at this point, based on the shape of the welding seam and the presence of local high-speed diffusion. The wide middle section of the weld could be explained by the overreaction between the middle section of the filler and base metals, due to the heat generated by the current. The high-speed diffusion at the ends of the cross-section proves that after the current had passed through the middle section of the seam, most of the current moved through the cross-section at both ends because of the skin effect produced by the current.

To prevent excessive filler metal outflow from the seam and observe the morphology of the filler metal

microstructure resulting from the welding process, a joining surface of the lower base metal was designed featuring 0.15 mm grooves. Figures 7(a−e) illustrate the microstructures of the joints obtained under condition IV. The filler metal was observed to fully connect with the lower base metal, but to only weakly connect with the upper base metal. As depicted in Fig. 7(f), the softening filler metal sections were closely contacted with the lower base metal under a larger pressure. Under the same current conditions, the heat at locations I (between the filler metal and the lower base metal) and II (between the filler metal and the upper base metal) was much higher than that generated by the material itself. The heat generated by the current softened the filler metal, which filled the grooves. And then the filler metal reacted with the base metal, which reduced the thickness of the filler metal and prevented it from filling the grooves. Furthermore, under the action of gravity and assisted by the good contact conditions obtained in the first stage, the filler metal reacted preferentially with the lower base metal. Figures 7(b, c) show magnifications of the images of zones *B* and *C* shown in Fig. 7(a), respectively. The filler metal is shown to be divided into three parts; the ends of the metal mainly consist of primary Al phase dendrites and some Al−Si−Mg eutectic regions, while the middle part of the filler metal is composed of spherical primary Al phase particles and small Al−Si−Mg eutectic regions. The observed morphology of the filler metal microstructure and the occurrence of holes in the middle section of the filler metal demonstrate that the filler metal on both ends melted, while the filler material in the middle section did not reach its melting point during the welding process. A high magnification image of zone *D* (Fig. 7(a)) shown in Fig. 7(d) reveals that the oxide film on the surface of the base metal and the unmolten filler metal was largely removed. Furthermore, the interface between the filler metal and the lower base metal contained a small number of pores, but there was only a weak connection between the filler metal and the upper base metal. When the solid and liquid phases of the same material coexist, the solid phase will act as the priority current channel owing to the significantly higher resistivity of the liquid metal phase [24]. Owing to the changing filler metal resistivity, as the current flows through both sides of the filler metal, it will preferentially move through the unmelted filler metal after the filler metal on both sides has melted. The weak contact between the unmolten filler metal and the upper base metal then becomes the current path. Figure 7(e) depicts the microstructure of the holes in the unmelted filler metal. Considering the entire resistance brazing process, the holes are found to result from the heat generated by the initial currents of the first and second stages. The current caused some filler metal to vaporise, which explains why the regions between the holes in the unmelted filler metal and upper base metal are better connected. The interface forms a metallurgical connection for the second step of the resistance brazing process, which uses a higher electrical energy input.

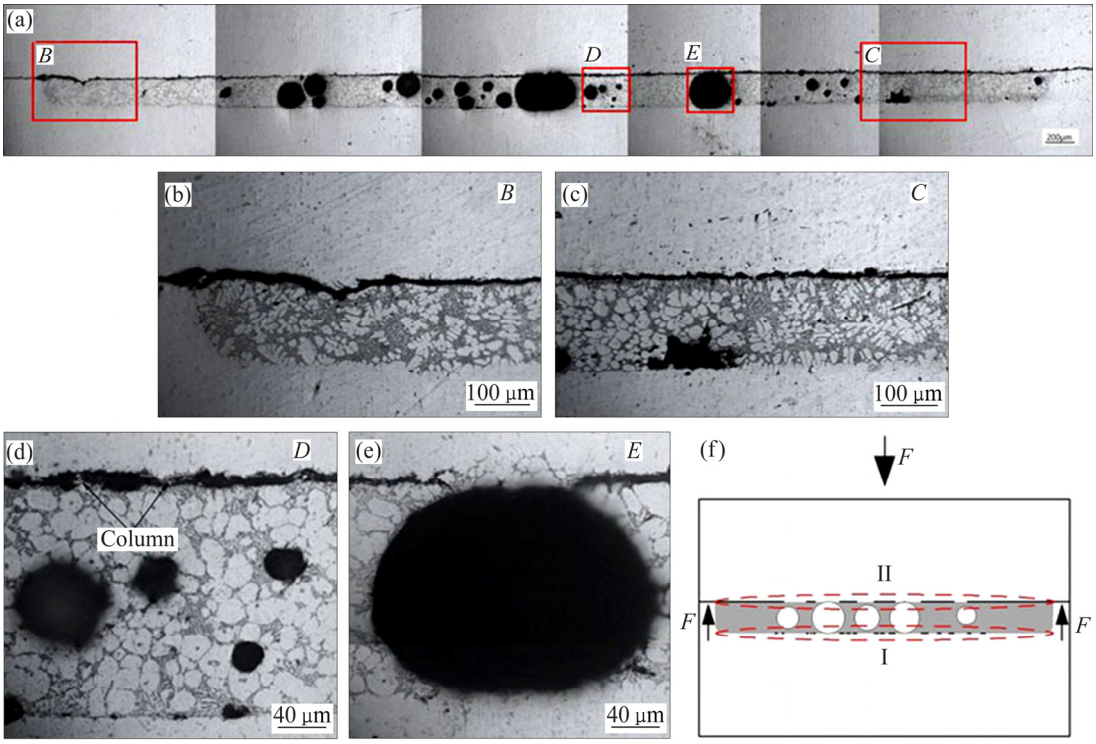

Fig. 7 OM images of resistance brazing welded joint under condition IV: (a) Microstructure of bonds; (b−e) Local magnification of zones *B*−*E* in (a), respectively; (f) Simple model

Increasing the duration of the second step caused the burst phenomenon to occur and a large amount of filler metal to be squeezed out of the seam. Figure 8 shows the joint microstructure of the grooved joint under condition V. Figure 8(a) shows that a large amount of molten filler metal and part of the base metal were squeezed out of the seam on the right side of the joint and formed a gap due to the burst phenomenon. The base metal on the left side of the cross-section was connected by metal columns. The high magnification image of zone *B* shown in Fig. 8(b) shows that the microstructure in the middle of the joint was mainly composed of primary Al phase dendrites and Al−Si−Mg eutectic regions.

EDS maps of the microstructure in the right side of the joint are shown in Figs. 8(d, e). The images show that Si in the base metal (which was connected by metal columns) diffused along the Al grain boundaries. The Si content of the local diffusion area (measured using EDS) was as high as 10.3%, which is much higher than that of the 0.4% Si in the parent metal. Therefore, it can be determined that diffusion of the Si also occurred from the filler metal to the base metal. After the filler metal was completely melted, most of the current selected a path along the edge of the groove joint. Because the edge is narrow, when the current was added to the molten filler metal of the high resistivity, it produced more heat. Under the action of the continuous current, the heat promoted rapid Si diffusion along the Al grain boundaries over a short time period, and the Al in the filler metal and the dissolution of Al in the base metal facilitated the formation of the metal columns.

Figure 9 illustrates the microstructure of the joint obtained under condition VI. Many cavities can be observed, and numerous fractures are visible in the base metal of the joint. The micrographs also show that the oxide film on the surface of the base metal and filler metal was substantially removed under the AC electric field, and that the melting filler metal reacted with the base metal sufficiently. The Al alloy on both sides was connected by metal columns composed of Al grains,

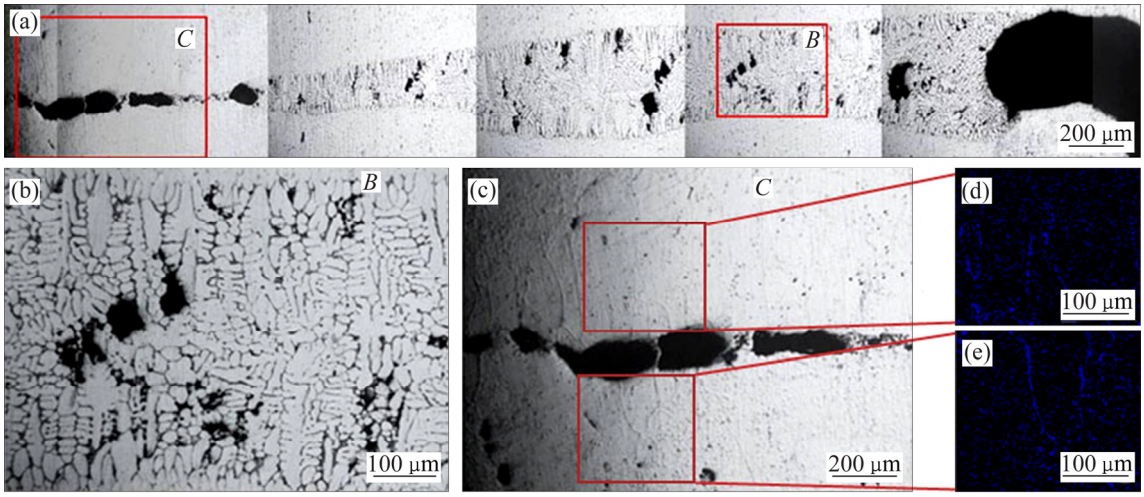

Fig. 8 OM images of resistance brazing welded joint under condition V: (a) Microstructure of bonds; (b, c) Local magnification of zone *B*, *C* in (a), respectively; (d, e) Corresponding EDS maps of Si in (c)

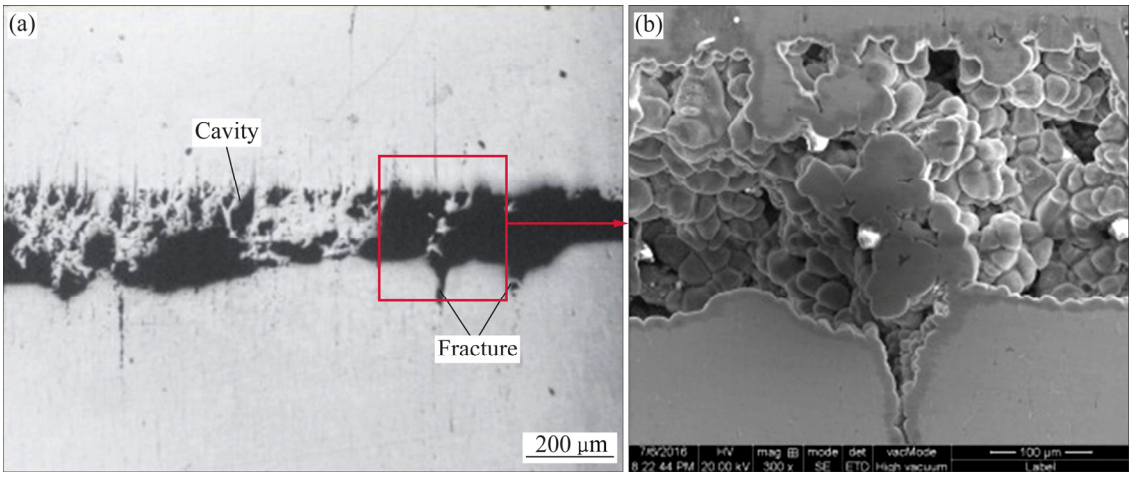

Fig. 9 OM and SEM images of resistance brazing welded joint under condition VI: (a) Microstructure of bonds; (b) Local magnification of zone in (a)

which contained a large number of cavities at their grain boundaries. The metal columns in the brazing seam consisted of irregular spherical and columnar aluminium (Fig. 9(b)).

3.2 Elimination of burst phenomenon

Applying ultrasonic vibration in a certain direction can eliminate the occurrence of the burst phenomenon in resistance brazing. Moreover, the welding joint geometry influences the duration of the ultrasonic vibration required to eliminate the burst. As shown in Fig. 10(a), an ultrasonic treatment was applied to the planar surface-welded joint at a horizontal horn position in the front of the sample, installed 5 mm from the joint. Despite the application of ultrasonic treatments for 2, 4, 6, and 10 s, the burst phenomenon was found to remain during the second resistance brazing stage.

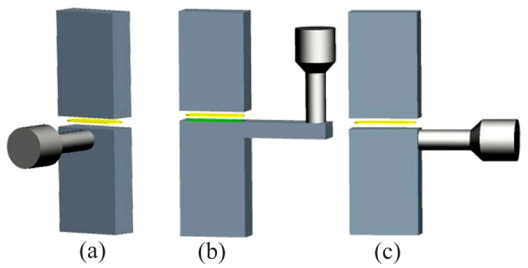

Fig. 10 Schematic of ultrasonic treatment applied in different directions

Ultrasonic treatments for 2, 4, 6, and 10 s were also vertically applied to the welded planar joint via a 5 mm-thick perpendicular beam (Fig. 10(b)). The burst phenomenon was found to remain after ultrasonic treatments for 2 and 4 s, but was eliminated after treatments for 6 and 10 s. However, in the welded groove joints the burst phenomenon only remained after 2 s of ultrasonic treatment, and was eliminated after treatment for 4 s or longer. Similarly, ultrasonic treatment was applied to the welded planar joint at a horizontal horn position on the side of the sample, installed 5 mm from the welded joint (Fig. 10(c)). The burst phenomenon remained after ultrasonic treatments for 2 and 4 s, but disappeared after 6 and 10 s treatments. In comparison, the burst phenomenon was observed in the welded groove joint after an ultrasonic treatment for 2 s, but was eliminated after 4, 6, and 10 s treatments.

Figure 11 shows the microstructure of the joint obtained under condition Ⅵ, combined with an ultrasonic treatment for 6 s. The brazed joint was found to exhibit a higher bonding ratio, and only a small number of unfilled holes and shrinkage holes were produced in the weld after cooling. The microstructure of the ultrasonic-assisted weld joint was composed of α(Al) solid solution vertical interface growth (appearing as light grey in the micrographs), Al−Si−Mg eutectic regions (black) and Si (dark grey), and acicular Si located at the eutectic and Al grain boundaries (Figs. 11(a) and (b)).

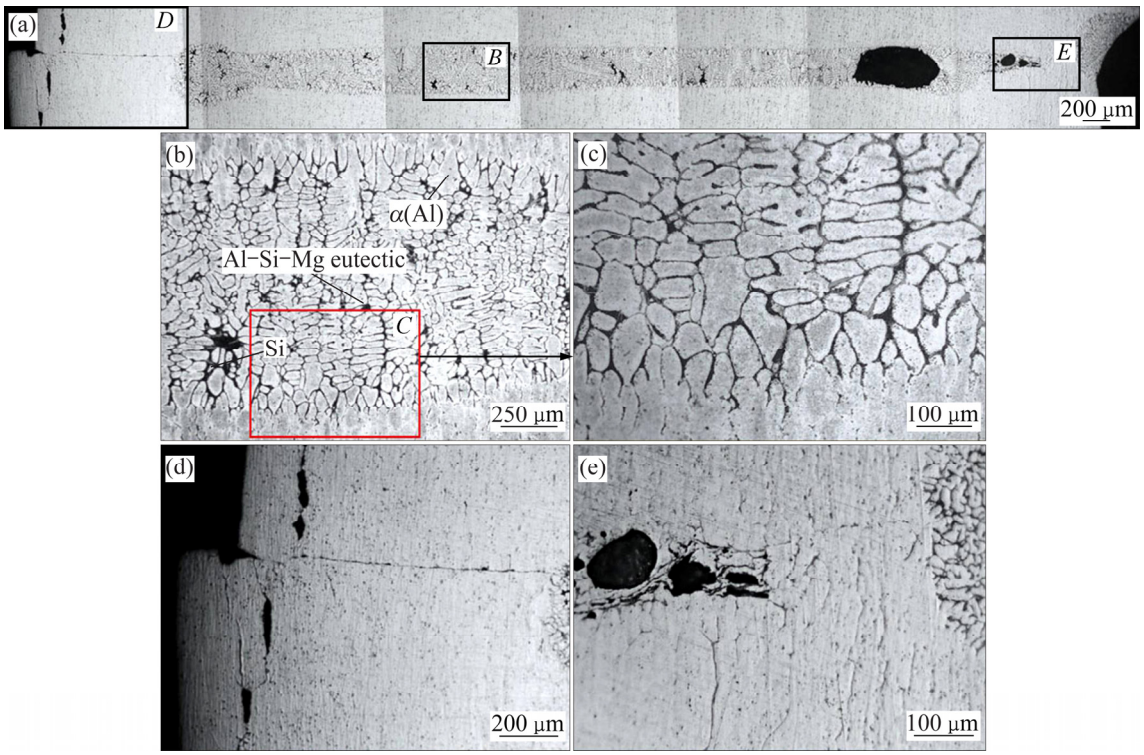

Fig. 11 OM images of resistance brazing welded joint under condition VI with ultrasonic treatment for 6 s: (a) Microstructure of bonds; (b−e) Local magnification of zones *B*, *D*, *E* in (a), respectively

Figures 11(d, e) show that the oxide film at the two ends of the cross-section is essentially removed. At this point, the two ends of the cross-section became the preferred current path owing to the skin effect and no high-resistivity oxide film to obstruct the current. The images also clearly indicate that the large amplitude of the current flowing through the ends of the cross-section produced a higher localised heating effect. This heat caused Si in the filler metal to diffuse along the high-rate diffusion channels (Al grain boundaries in the parent material) [25]. The continuous current subsequently caused the heat in the local area to become too high, resulting in excessive Si reaction and diffusion to the base material. In this way, corrosion occurred and produced holes. Through this process, a large current flow through the molten filler metal is avoided, and thus, burst caused by a high current density in the local liquid filler metal is prevented.

3.3 Mechanism of ultrasonic-assisted resistance brazing

Schematics summarizing the ultrasonic-assisted resistance brazing process in different joining surface geometries are depicted in Fig. 12 to further illustrate the burst production and elimination mechanism. The white regions represent the Al substrate, the Al−Si−Mg solid filler metal appears in light grey regions, the dark grey regions indicate the Al−Si−Mg liquid phase or the coexistent form of the solid phase and molten filler metal, and the black regions represent the filler metal after solidification. The red lines indicate the current path; thin lines represent the path of the smaller current, dotted lines represent the previous current path, and thick lines represent the path of the larger current. The ultrasonic-assisted resistance brazing process was divided into two steps. Figures 12(a_1, a_2) depict the first welding step for joints with planar and grooved joining surfaces, respectively. Figures 12(b_1, b_2) show the initial second step applied to a welded planar and groove, respectively. Most of the current preferentially selected a new path through both ends of the cross-section (the red lines) because of the skin effect. The burst phenomenon occurred in the liquid filler metal (see Figs. 12(c_1, c_2)). However, excessive reaction of the filler metal with the base metal caused expansion, contraction, and solidification of the melted filler metal to occur, producing new holes in the filler metal. After cooling and solidification, the dissolution of a large amount of filler metal into the Al substrate at both ends caused many holes to form in the brazing seam (Figs. 12(d_1, d_2)).

Figure 12(b_3) shows the second ultrasonic-assisted resistance brazing step applied to a welded groove joint in combination with ultrasonic vibration. Ultrasonic treatment accelerated the removal of the oxide film and played an important role in the stirring of the melted filler metals (Fig. 12(c_3)). At this point in the process, most of the current preferentially selected a path through the ends of the cross section of the base metal (red lines), preventing a large current flow through the melted filler metal and eliminating the burst phenomenon. After

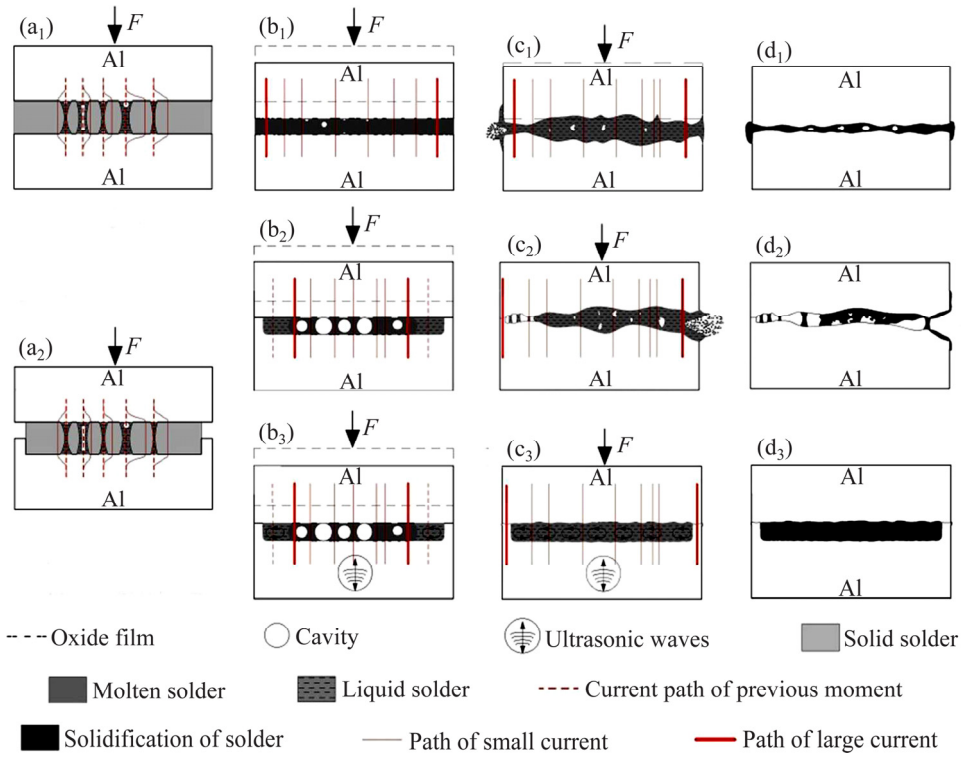

Fig. 12 Schematics of ultrasonic-assisted resistance brazing process with different joining surface geometries

solidification, an excellent weld was obtained (Fig. 12(d_3)). However, when the oxide film on the edge of the cross-section of the two parent metals was not removed after the ultrasonic vibration was applied. As a result, the burst phenomenon was not eliminated.

4 Conclusions

(1) A two-step ultrasonic welding method and its associated apparatus are developed to make Al alloy joints. In this method, ultrasonic-assisted resistance brazing is divided into two steps. The instantaneous large current (the initial currents of the first and second stages) formed a metallurgical connection at the interface, and improved contact conditions between the base and filler metals. The higher current of the second step melted the filler metal.

(2) The ultrasonic direction and time, as well as the welding joint geometry, have great effects on the formation and elimination of burst phenomenon. Ultrasonic treatments with greater than or equal to 6 s are vertically applied to the welded planar joint, and finally the burst phenomenon is eliminated. It is more effectively to eliminate the burst phenomenon with 4 s through adding a groove joints with a size of 0.15 mm.

(3) A model has been presented for the whole process including the formation and elimination of the burst phenomenon and the variation rule of the current path.

References

[1] JI Hong-jun, LI Ming-yu, LU Yong-fei, WANG Chun-qing. Mechanical properties and microstructures of hybrid ultrasonic resistance brazing of WC-Co/BeCu [J]. Journal of Materials Processing Technology, 2012, 212(9): 1885−1891.

[2] TAKESHITA K, TANAKA H. Microjoining of stainless steel using two-step resistance brazing method [J]. Quarterly Journal of the Japan Welding Society, 2007, 25(1): 45−50.

[3] XUE Song-bai, LV Xiao-chun, ZHANG Hui-wen. Resistance brazing technology of TiNi shape memory alloy [J]. Transactions of the China Welding Institution, 2004, 25(1): 1−4. (in Chinese)

[4] TANAKA Y, YAMAGUCHI T, TAKESHITA K. Numerical simulation of joining during the two-step resistance brazing [J]. Welding International, 2013, 27(11): 857−866.

[5] WIELAGE B, HOYER I, WEIS S. Combined ultrasonic resistance brazing of aluminium [J]. Materials Science and Materials Engineering, 2010, 41(9): 802−806.

[6] WEIS S, WIELAGE B, SEEHOFER C. Ultrasound-assisted resistance soldering of aluminium matrix composites [J]. Materials Science and Materials Engineering, 2012, 43(7): 656−660.

[7] LAMPKE T, WIELAGE B, HOYER I, KÜMMEL S, PISCHTCHAN M. Ultrasound-assisted resistance brazing of magnesium and aluminium alloys using melt-spin solder foils [C]//Proceedings of the 5th International Brazing and Soldering Conference. Las Vegas, U.S.: ASM International, 2012: 389−393.

[8] FLOREA R, BAMMANN D, YELDELL A, SOLANKI K, HAMMI Y. Welding parameters influence on fatigue life and microstructure in resistance spot welding of 6061-T6 aluminum alloy [J]. Materials & Design, 2013, 45: 456−465.

[9] ZHENG Zhen-tai, SHAN Ping, HU Sheng-sun, LUO Zhen. Resistance spot welding of aluminum alloy with great resistance medium [J]. Transactions of the China Welding Institution, 2006, 27(7): 5−8. (in Chinese)

[10] GUO Wei-bing, LUAN Tian-min, LENG Xue-song, HE Jing-shan, YAN Jiu-chun. Interfacial microstructure evolution and mechanical properties of Al/Sn joints by ultrasonic-assisted soldering [J]. Transactions of Nonferrous Metals Society of China, 2017, 27(4): 962−970.

[11] ATAMANENKO T, ESKIN D, ZHANG L, KATGERMAN L. Criteria of grain refinement induced by ultrasonic melt treatment of aluminum alloys containing Zr and Ti [J]. Metallurgical & Materials Transactions A, 2010, 41(8): 2056−2066.

[12] PATEL B, CHAUDHARI G, BHINGOLE P. Microstructural evolution in ultrasonicated AS41 magnesium alloy [J]. Materials Letters, 2012, 66(1): 335−338.

[13] CHINNAM R, FAUTEUX C, NEUENSCHWANDER J, JANCZAK-RUSCH J. Evolution of the microstructure of Sn–Ag–Cu solder joints exposed to ultrasonic waves during solidification [J]. Acta Materialia, 2011, 59(4): 1474−1481.

[14] XIAO Yong, JI Hong-jun, LI Ming-yu, KIM J, KIM H. Microstructure and joint properties of ultrasonically brazed Al alloy joints using a Zn–Al hypereutectic filler metal [J]. Materials & Design, 2013, 47(9): 717−724.

[15] LI Yuan-xing, ZHAO Wei-wei, LENG Xue-song, FU Qiu-jiao, WANG Lei, YAN Jiu-chun. Microstructure evolution and mechanical properties of ultrasonic-assisted soldering joints of 2024 aluminum alloys [J]. Transactions of Nonferrous Metals Society of China, 2011, 21(9): 1937−1943.

[16] BELOVA V, SHCHUKIN D G, GORIN D A, KOPYSHEV A, MÖHWALD H. A new approach to nucleation of cavitation bubbles at chemically modified surfaces [J]. Physical Chemistry Chemical Physics, 2011, 13(17): 8015−8023.

[17] SKORB E V, SHCHUKIN D G, MÖHWALD H, ANDREEVA D. Ultrasound-driven design of metal surface nanofoams [J]. Nanoscale, 2010, 2(5): 722−727.

[18] DULAR M, DELGOSHA O, PETKOVŠEK M. Observations of cavitation erosion pit formation [J]. Ultrasonics Sonochemistry, 2013, 20(4): 1113−1120.

[19] LENG Xue-song, WANG Chang-wen, ZHANG Yang, CHEN Xiao-guang, YAN Jiu-chun. Strengthening mechanism of ceramic particle reinforced bonds by ultrasonic brazing of AlMMCs [J]. Transactions of Nonferrous Metals Society of China, 2011, 21(s2): s290−s294.

[20] MA Zhi-peng, ZHAO Wei-wei, YAN Jiu-chun, LI Da-cheng. Interfacial reaction of intermetallic compounds of ultrasonic-assisted brazed joints between dissimilar alloys of Ti4V and Al1Mg [J]. Ultrasonics Sonochemistry, 2011, 18(5): 1062−1067.

[21] CUI Y, XU C, HAN Q. Effect of ultrasonic vibration on unmixed zone formation [J]. Scripta Materialia, 2006, 55(11): 975−978.

[22] NIU Zhi-wei, HUANG Ji-hua, CHEN Shu-hai, ZHAO Xing-ke. Effects of germanium additions on microstructures and properties of Al−Si filler metals for brazing aluminium [J]. Transactions of Nonferrous Metals Society of China, 2016, 26(3): 775−782.

[23] JI Chun-tao. Welding manual: Welding methods and equipment [M]. Beijing: Mechanical Industry Press, 2007: 407−425. (in Chinese)

[24] SHIMOJI M. Liquid metals [M]. GUO J, ed. Beijing: Academic Press, 1987: 313−324. (in Chinese)

[25] PORTER D, EASTERLING K, SHERIF M. Phase transformation in metals and alloys [M]. CHEN L, YU Y, ed. Beijing: Higher Education Press, 2011: 84−86. (in Chinese)

超声辅助电阻钎焊中爆破现象的形成与消除

俞伟元[1]，张天宇[1,2]，王 玉[2]，高盟召[1]，尚江旭[1]，颜泽华[1]，吴炜杰[1]，林巧力[1]

1. 兰州理工大学 有色金属先进加工与再利用国家重点实验，兰州 730050；
2. 东北大学 轧制与自动化国家重点实验室，沈阳 110819

摘　要：使用两步超声波钎焊方法及其相关装置，采用 Al−Si−Mg 钎料对 6063 铝合金进行超声辅助电阻钎焊。研究爆破现象以及超声波的方向、时间和焊接接头几何形状对爆破现象的影响。结果表明：在高电流密度、高热量和相互作用力的共同作用下，液态钎料发生了爆破现象。超声波的方向和时间以及焊缝几何形状对爆破现象有显著影响。当超声波时间不小于 6 s 时，可以去除母材表面的氧化膜，消除爆破现象。提出描述爆破形成和消除的模型，且通过改变超声时间和焊接接头几何形状来控制爆破现象。

关键词：6063 铝合金；超声辅助钎焊；电阻钎料；爆破

(Edited by Xiang-qun LI)